We are IntechOpen, the world's leading publisher of Open Access books Built by scientists, for scientists

5,000
Open access books available

125,000
International authors and editors

140M
Downloads

Our authors are among the

154
Countries delivered to

TOP 1%
most cited scientists

12.2%
Contributors from top 500 universities

WEB OF SCIENCE™

Selection of our books indexed in the Book Citation Index in Web of Science™ Core Collection (BKCI)

Interested in publishing with us?
Contact book.department@intechopen.com

Numbers displayed above are based on latest data collected.
For more information visit www.intechopen.com

Chapter

Extracting Coherent Structures in Near-Wall Turbulence Based on Wavelet Analysis

Peng Du, Haibao Hu and Xiao Huang

Abstract

To analyze the properties of the coherent structures in near-wall turbulence, an extraction method based on wavelet transform (WT) and a verification procedure based on correlation analysis are proposed in this work. The flow field of the turbulent boundary layer is measured using the hot-film anemometer in a gravitational low-speed water tunnel. The obtained velocity profile and turbulence intensity are validated with traditional boundary layer theory. The fluctuating velocities at three testing positions are analyzed. Using the power spectrum density (PSD) and WT, coherent and incoherent parts of the near-wall turbulence are extracted and analyzed. The probability density functions (PDFs) of the extracted signals indicate that the incoherent structures of turbulence obey the Gaussian distribution, while the coherent structures deviate from it. The PDFs of coherent structures and original turbulence signals are similar, which means that coherent structures make the most contributions to the turbulence entrainment. A correlation parameter is defined at last to prove the validity of our extraction procedure.

Keywords: coherent structure, wavelet transform, correlation analysis, turbulence

1. Introduction

Turbulence is a commonly seen but very complicated phenomenon in nature. Numerous tests have proven that turbulence is not a pure random process but contains different scales of fluctuations called coherent structures [1–3]. These structures significantly contribute to fluid entrainment and mass, momentum, and heat transfer [4, 5]. Therefore, investigating the coherent structures is of great significance to undercover the physics and to realize flow control.

Among the techniques of turbulence analysis, wavelet transform has been proven feasible and power to detect and extract the coherent structures in turbulence [6–9]. Early works are based on continuous wavelet transform (CWT). Liandrant [10] and Jiang [11, 12] proposed the maximum energy principle, which considered the signal at the maximum energy scale as the burst events in turbulence. Kim [13] identified the coherent structure around a vibrating cantilever based on CWT. However, a drawback of CWT is that it is unable to reconstruct the signal if the mother wavelet is not orthogonal [14–16]. To solve this problem, Longo [17] used the multiresolution analysis technique based on the discrete wavelet transform (DWT) and extracted the structures in turbulence. DWT has evident

advantages compared with CWT since it is invertible and multi-scaled scales can be analyzed. Kadoch [18] combined DWT and direct numerical simulation (DNS), whose results proved that coherent structures preserve the vortical structures with only about 4% of the wavelet coefficients but retain 99.9% of the turbulence energy.

In this work, measurement of the turbulent boundary layer is carried out using hot-film anemometer in a gravitational low-speed water tunnel. A procedure based on the WT and correlation analysis is proposed to extract and verify the coherent and incoherent structure in turbulence.

2. Experimental tests and analysis

2.1 Experimental apparatus

A gravitational low-speed water tunnel was constructed for the experiment. The gravity generated by the water level difference drives the water flow in the tunnel, and the flow can be tested in the experimental section (**Figure 1**). A maximum water speed of 2.0 m/s can be reached, and the turbulence intensity is less than 2%. The IFA300 hot-wire anemometer was used to measure the turbulence boundary layer flow at a series of positions in the vertical direction (**Figure 2**). Detailed setups in the experimental section can be observed in **Figure 2**. A probe penetrates into the

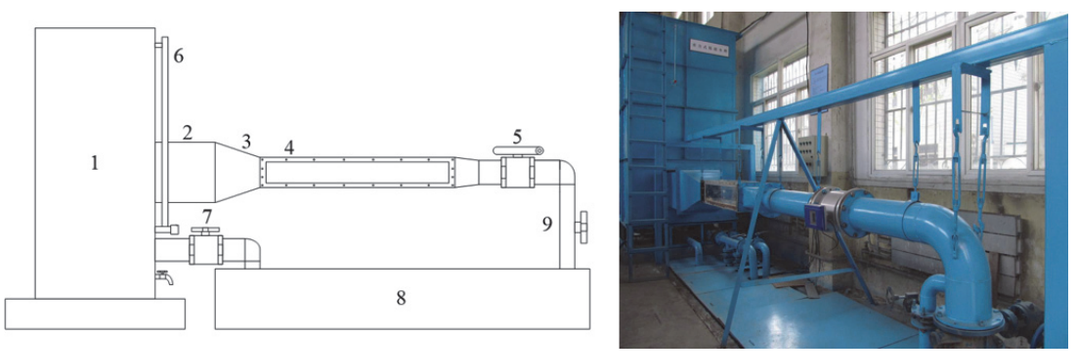

Figure 1.
Sketch (left) and photo (right) of the gravitational low-speed water tunnel. (1) Water tank; (2) stabilization section; (3) contraction section; (4) experimental section; (5) electromagnetism flowmeter; (6) water level observation section; (7) water pump; (8) water storage basin; (9) switch valve.

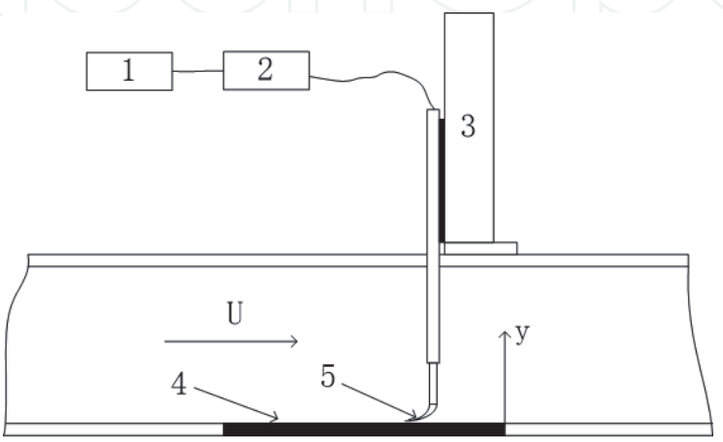

Figure 2.
Sketch of experimental setups. (1) PC; (2) hot-film anemometer; (3) coordinate frame; (4) experimental plate; (5) hot-film probe.

flow to measure the flow field. A coordinate frame was used to move the probe in the vertical direction, with a precision of 0.01 *mm*. During the experiment, the sampling frequency and sampling time were set to 50 *kHz* and 10.24 *s*.

2.2 Verification of turbulent boundary layer flow

By using the experimental setups in **Figure 2**, the flow velocity of the turbulence boundary layer was measured at a series of positions in the vertical direction. The mean velocity profile and the turbulence intensity distribution at the water speed 0.4 *m/s* can are analyzed in **Figures 3** and **4**, which agree with the turbulence boundary

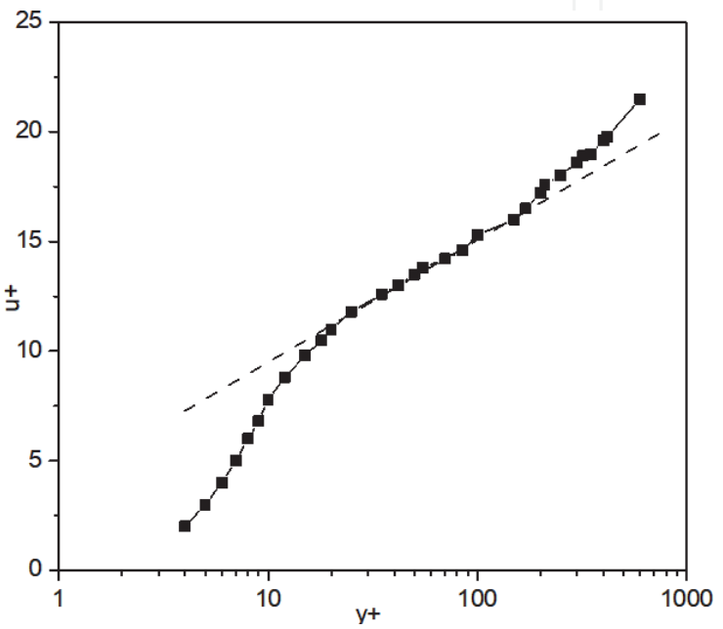

Figure 3.
The profile of mean velocity at the water speed 0.4 m/s.

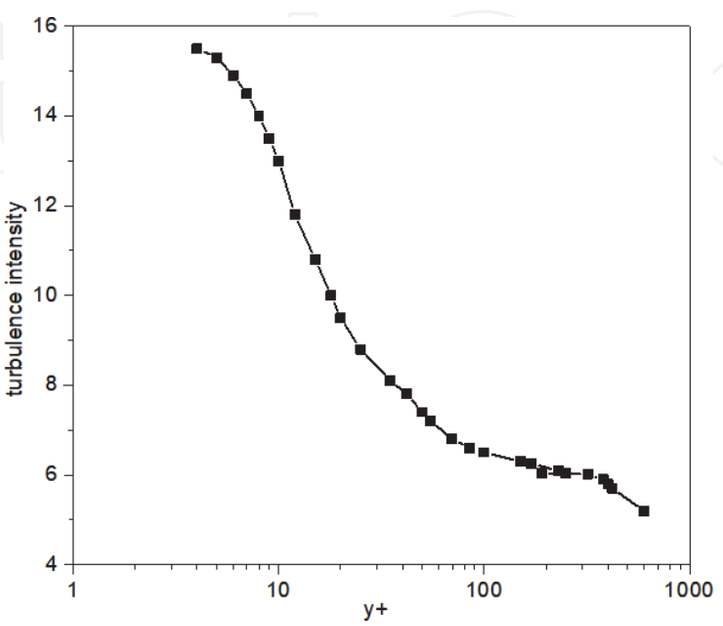

Figure 4.
Turbulence intensity at the water speed 0.4 m/s.

layer theory. This means that the flow field in the experimental section is fully developed. Our setups and techniques are ready for turbulent boundary layer tests.

3. Theoretical background of wavelet transform

WT is a mapping of a time function, in a one-dimensional case, to the two dimensional time-scale joint representation. The temporal aspect of the signal can be preserved. The wavelet transform provides multiresolution analysis with dilated windows. The high-frequency part of the signal is analyzed using narrow windows, and the low-frequency part is done using wide windows. WT decomposes the signal into different frequency components and then studies each component with a resolution matched to its scale. It has advantages over traditional Fourier methods in analyzing physics where the signal contains discontinuities and sharp spikes.

WT of a signal $s(t)$ is defined as the integral transform of $\psi_{a,b} = \frac{1}{\sqrt{a}}\psi\left(\frac{t-b}{a}\right)$, which can be expressed as:

$$\begin{aligned} W_f(a,b) &= \int_{-\infty}^{\infty} s(t)\psi_{a,b}dt \\ &= \int_{-\infty}^{\infty} s(t)\frac{1}{\sqrt{a}}\psi\left(\frac{t-b}{a}\right)dt \end{aligned} \tag{1}$$

where $\varphi_{m,n}(t)$ is the scaling function, which is defined as $\varphi_{m,n}(t) = 2^{-m/2}\varphi(2^{-m}t - n)$, and where a and b are the scale and position [19].

Scale a and position b should be discretized for applications. Usually we choose $a = 2^m (m \in Z, a_0 > 1)$, $b = n \cdot 2^m (b_0 > 0, n \in Z)$. When $\psi(t)$ obeys the orthogonal condition $\int \psi_{m,n}(t)\psi_{m',n'}(t)dt = \delta_{m,m'}\delta_{n,n'}$, the functions of the orthogonal basis can be written as:

$$\begin{aligned} \psi_{m,n}(t) &= \frac{1}{\sqrt{2^m}}\psi\left(\frac{t - n\cdot 2^m}{2^m}\right) \\ &= 2^{-m/2}\psi(2^{-m}t - n) \end{aligned} \tag{2}$$

The corresponding DWT can be expressed as:

$$\begin{aligned} <s, \psi_{m,n}> &= 2^{-m/2}\int_{-\infty}^{\infty} s(t)\psi_{m,n}(t)dt \\ &= 2^{-m/2}\int_{-\infty}^{\infty} s(t)\psi(2^{-m}t - n)dt \end{aligned} \tag{3}$$

The orthogonality of $\psi_{m,n}(t)$ eliminates the relevance between the points in wavelet space because of redundancy. The analyzing result of WT can thus reflect the characteristics of the original signal. Based on OWT, the signal $s(t)$ can be written as:

$$s(t) = \sum_{-\infty}^{\infty}\sum_{-\infty}^{\infty} <s, \psi_{m,n}>\psi_{m,n}(t) \tag{4}$$

By choosing the scale m_0 as the critical value, the signal $s(t)$ can be divided into the approximate and detailed parts:

$$
\begin{aligned}
s(t) &= \sum_{m=m_0+1}^{\infty}\sum_{n=-\infty}^{\infty} <s,\psi_{m,n}>\psi_{m,n}(t) + \sum_{m=-\infty}^{m_0}\sum_{n=-\infty}^{\infty} <s,\psi_{m,n}>\psi_{m,n}(t) \\
&= \sum_{n=-\infty}^{\infty} <s,\varphi_{m,n}>\varphi_{m_0,n}(t) + \sum_{m=-\infty}^{m_0}\sum_{n=-\infty}^{\infty} <s,\psi_{m,n}>\psi_{m,n}(t) \\
&= \sum_{n=-\infty}^{\infty} a_{m_0}[n]\varphi_{m_0,n}(t) + \sum_{m=-\infty}^{m_0}\sum_{n=-\infty}^{\infty} d_m[n]\psi_{m,n}(t) \\
&= A_{m_0} + \sum_{m=1}^{m} D_m
\end{aligned}
\tag{5}
$$

where $\psi_{m,n}(t)$ is the wavelet function. $\varphi_{m,n}(t)$ can be viewed as a low-pass filter, while $\psi_{m,n}(t)$ as a band-pass filter. The first part of the above equation is the low-frequency approximation of the signal $s(t)$ at the scale 2^{-m0}; the high-frequency part is the details of the signal $s(t)$ [15, 20].

For turbulence, the fluctuating velocity of turbulence can be normally divided into two subparts:

$$s = \tilde{s} + s' \tag{6}$$

where $\tilde{s}$ is the coherent part and s' is the incoherent part. The signals $\tilde{s}$ and s' are statistically independent.

By adopting the multiresolution analysis (**Figure 5**), the turbulence signal $s(t)$ can be divided into different frequencies. Coherent structures can thus be reconstructed in a selected frequency domain. Other redundant signals can then be eliminated. Therefore, the frequency range determination and localization of the coherent structures are critical in this process. The frequency can be determined as:

$$f = \frac{f_c f_i}{a} \tag{7}$$

where f_s and f_c are the sampling frequency and the central frequency of a particular wavelet basis. a is the scale, denoted as 2^m (m is a particular level of decomposition) in OWT. It represents the original frequency range of the turbulence signal when $m = 0$ (i.e., $a = 1$), $f = f_0$.

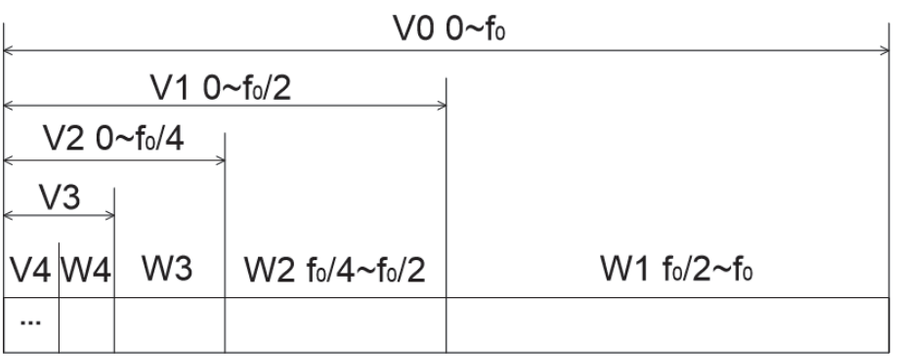

Figure 5.
Sketch of the multiresolution analysis.

4. Extraction and verification of turbulent structures

To extract the coherent structures in turbulence, the signals at the central area of turbulence should be selected. According to previous studies [20–22], the formation of the coherent structures in turbulence is formed in the area of $0 < y^+ < 30$, and the self-sustaining of the coherent structures is in the area of $20 < y^+ < 60$. As a result, three testing positions with the y^+ 20.8, 33.5, and 42.6 were selected, whose fluctuating velocity signals are shown in **Figure 6**.

4.1 Preliminary evaluation of coherent structures

For preliminary evaluations of the coherent structures, CWT is first utilized for the analysis. CWT is a mathematical mapping similar to the Fourier transform [23, 24]. It is linear, invertible, and orthogonal. However, the Fourier transform uses basis functions, including the sines and cosines, which extend to infinity in time, while wavelet basis functions drop towards zero outside a finite domain (compact support). This allows for an effective localization in both time and frequency. CWT uses inner products to measure the similarity between the turbulence signal and the wavelet function, which defines a mapping between the two. CWT compares the turbulence signal to shifted and compressed/stretched versions of the wavelet function. Compressing/stretching is also referred to as dilation or scaling and corresponds to the physical notion of scale. By continuously varying the values of the scale parameter, a, and the position parameter, b, one can obtain the CWT coefficients at last.

In the work, the 5th order of Daubechies wavelet was selected as the basis function, whose central frequency fc is 0.6667 *Hz*. The calculated CWT coefficients of the three signals are shown in **Figure 7**, where the quasi-periodic structures (coherent structures) of turbulence can be clearly observed. The modulus of the wavelet coefficients shows that during the vortex breakdown, which is caused by the strong nonlinear flow instability, energy is spread over a wide range of scales. Large-scale structures exhibit anisotropic properties in the flow. Their peaks and troughs appear at the scale about 300, corresponding with a frequency of 0.6667/300 = 0.0022 *Hz*. These dominant scales will have the highest level of energy in turbulence. At the smaller scales, the vortices break up into intermittent small-scale features. Some organizations are evident here, with periodical and intermittent turbulent bursts. The low-frequency structures will decay to isotropic structures and dissipate in turbulence at last.

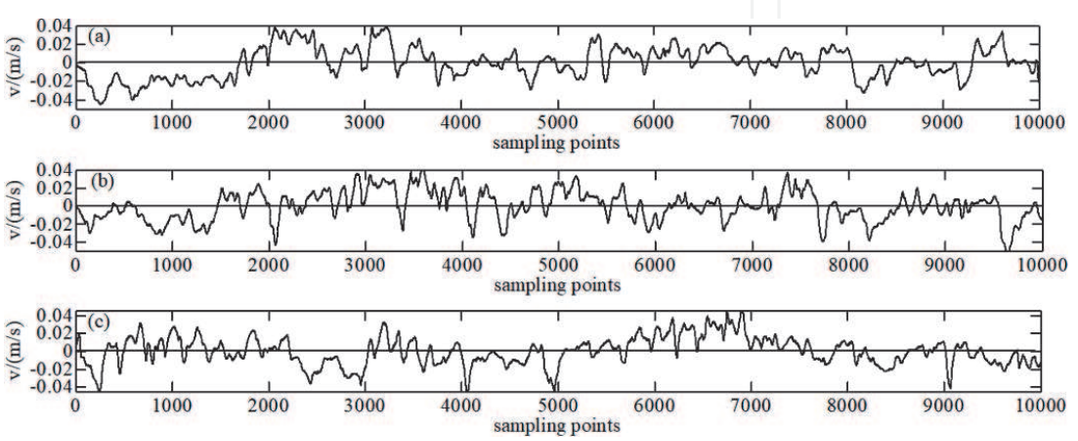

Figure 6.
Fluctuating velocity signals at three positions (a) $y^+ = 20.8$, (b) $y^+ = 33.5$, (c) $y^+ = 42.6$.

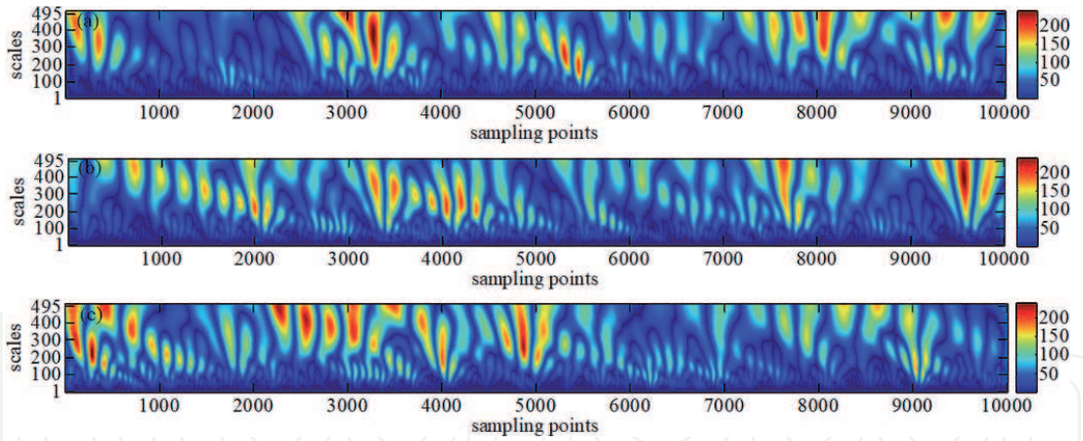

Figure 7.
Continuous wavelet transform coefficients at (a) $y^+ = 20.8$, (b) $y^+ = 33.5$, (c) $y^+ = 42.6$.

4.2 Extraction of coherent structures

To obtain the frequency range of coherent structures in turbulence, power spectrum densities of the three selected signals were calculated in **Figure 8**. The centralized frequencies of the coherent structures are found in the range $0 \sim 230$ *Hz*, $0 \sim 240$ *Hz*, $0 \sim 230$ *Hz*. The rapid attenuation of PSD demonstrates the low noise of our experimental system. Multiresolution analysis of OWT was used to extract the coherent structures in turbulence [9, 25, 26].

WT of a signal is equivalent to local cross-correlation analysis between the signal and wavelet function. OWT carries out the multi-resolution analysis for both decomposition and reconstruction of the original turbulence signal. It is thought of the wavelet coefficients as digital filters as which the original signal is passed through low-pass filters to decompose into low-frequency components and passed through high-pass filters to analyze into high-frequency components.

Using the multiresolution analysis of OWT, the turbulence signal was split into seven scales as in **Table 1**, which eliminates most of the redundant signals. The frequency range of the approximate signal is mainly in the range $0 \sim 260$ *Hz*, which covers most of the coherent structures. In **Table 1**, the coherent structures are found to take almost 75 % of the whole energy in turbulence.

The extracted signals of each level are shown in **Figure 9**, where "A7" is the approximate signal, i.e., the coherent structures; where "sD7" is the incoherent structures, which is calculated by:

$$\mathrm{sD7} = \mathrm{s} - \mathrm{A7} = \mathrm{D1} + \mathrm{D2} + \cdots + \mathrm{D7}, \tag{8}$$

and where "s" is the original signal. "D1 ∼ D7" are the detailed signals of each level.

4.3 Verification of extracted signals

To characterize the properties of the extracted signals, the probability density functions (PDFs) were analyzed in **Figure 10**. It can be observed that the incoherent structures are approximately Gaussian, demonstrating isotropic characteristics. The PDFs of coherent structures deviate from the Gaussian distribution, presenting strong anisotropic characteristics. And the PDFs of the coherent structures resemble that of the original turbulence signals. This means that coherent structures contribute the most to turbulence entrainment.

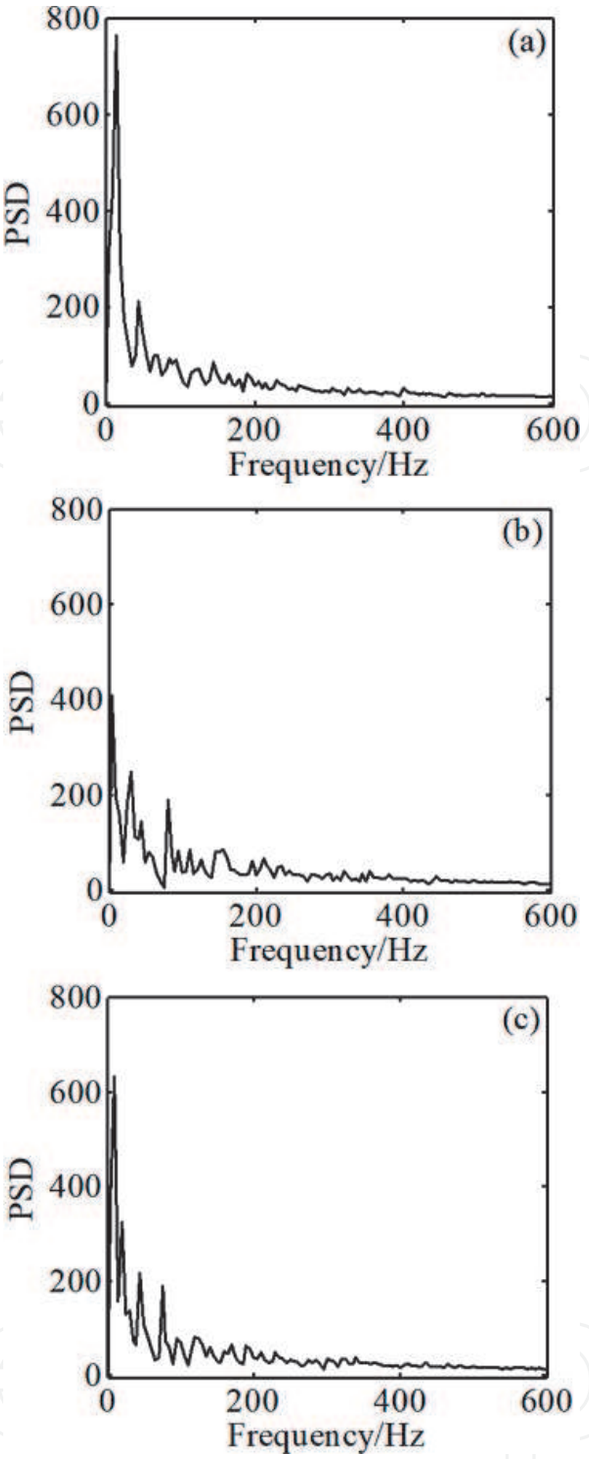

Figure 8.
Power spectrum densities at the three positions (a) $y^+ = 20.8$, (b) $y^+ = 33.5$, (c) $y^+ = 42.6$.

For further validation of the extracted coherent and incoherent structures, correlation analysis was carried out here. A correlation parameter β between these structures was defined [27]:

$$\beta = \frac{\overline{v_a v_d}}{\overline{v^2}} = \frac{\frac{1}{N}\sum v_{ai} v_{di}}{\frac{1}{N}\sum v_i^2} \tag{9}$$

where v is the fluctuating velocity signal. The subscripts "a" and "d" represent the coherent and incoherent structures. N is the number of the sampling points. $\overline{v_a v_d}$ can be regarded as the stress between the coherent and incoherent structures.

Signal	Frequency/*Hz*	Energy/%		
		$y^+ = 20.8$	$y^+ = 33.5$	$y^+ = 42.6$
s	0 ~ 33,335	100	100	100
*A*7	0 ~ 260	85.6498	77.0677	81.3847
*D*7	260 ~ 520	0.0147	0.0200	0.0259
*D*6	520 ~ 1042	0.0062	0.0086	0.0129
*D*5	1042 ~ 2083	0.0019	0.0036	0.0042
*D*4	2083 ~ 4167	0.0464	0.0703	0.0868
*D*3	4167 ~ 83,334	0.3957	0.8099	0.8505
*D*2	83,334 ~ 16,668	3.5993	5.5974	5.2322
*D*1	16,668 ~ 33,335	10.2411	16.4225	12.4028

Table 1.
Frequency and energy distribution of seven level decompositions.

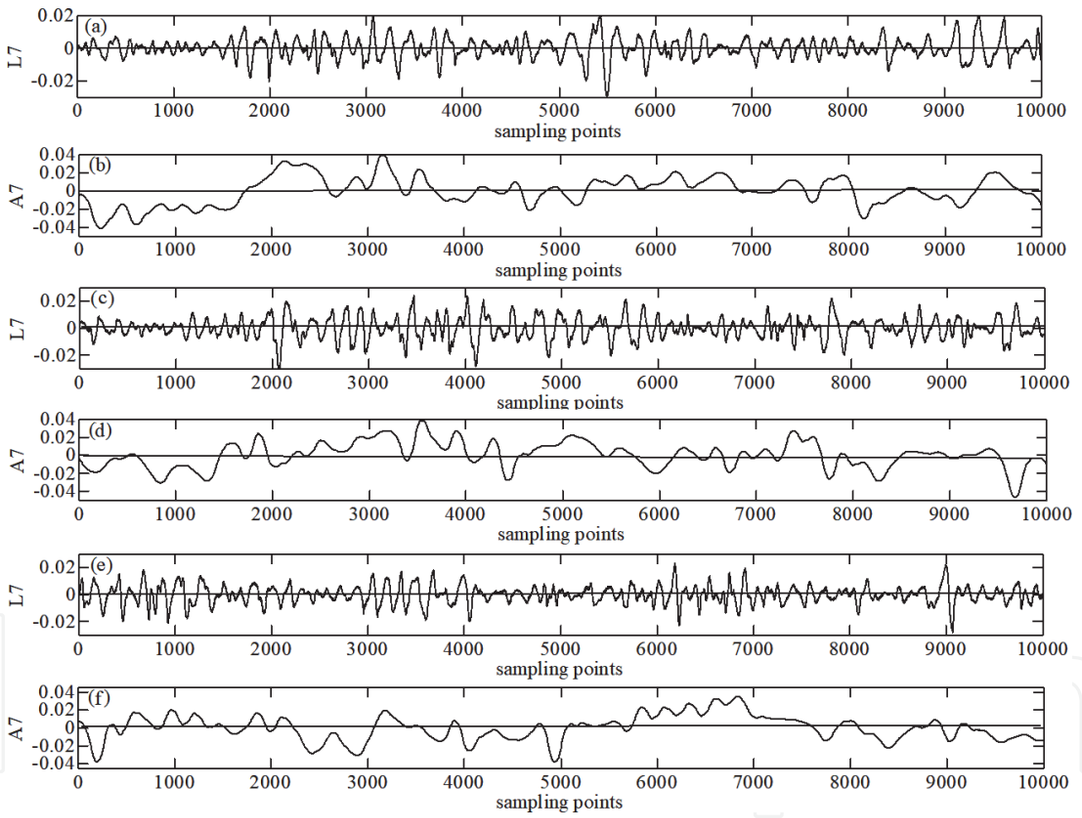

Figure 9.
Extracted signals in turbulence. (a) Incoherent structure ($y^+ = 20.8$); (b) coherent structure ($y^+ = 20.8$); (c) incoherent structure ($y^+ = 33.5$); (d) coherent structure ($y^+ = 33.5$); (e) incoherent structure ($y^+ = 42.6$); (f) coherent structure ($y^+ = 42.6$).

Value of β represents the correlation between coherent and incoherent structures. A large value of β means that the coherent structures are divided into detailed signals as incoherent structures, denoting an inappropriate selection of the decomposition level. If the coherent structures are correctly extracted, the correlation parameter β should be 0. According to Eq. (9), β of our three selected signals at the level 7 are -3.8444×10^{-4}, 7.2638×10^{-4}, and 3.2677×10^{-4}, respectively, demonstrating the low correlation between the extracted coherent and incoherent structures. This proves the validity of the proposed extraction process.

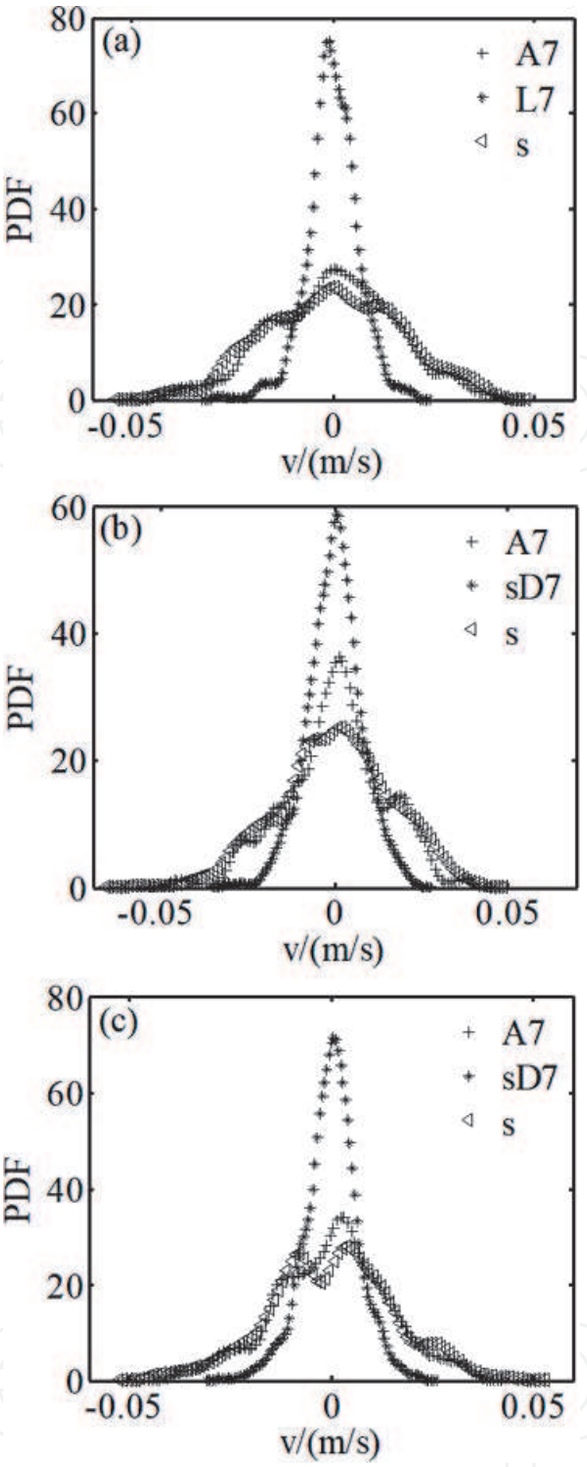

Figure 10.
Probability density functions at three testing positions (a) $y^+ = 20.8$, (b) $y^+ = 33.5$, (c) $y^+ = 42.6$.

5. Conclusion

The flow field of the turbulence boundary layer was measured using hot-film anemometer in a gravitational low-speed water tunnel. The coherent and incoherent structures in turbulence were separated successfully with an extraction method based on WT. With CWT, the turbulent structures can be observed in various scales. With DWT, multiresolution analysis can be carried out for the decomposition and reconstruction of vortical structures in different scales. The PDF of the incoherent structures was found to obey the Gaussian distribution, while that of the

coherent structures deviate from it. The similarity of the PDFs of the coherent structures and the original turbulence signal demonstrate that the coherent structures make most contributions to turbulence. A correlation parameter between coherent and incoherent structures was defined, which proves the successful separation of coherent structure from turbulence.

Acknowledgements

The authors acknowledge the support from the National Natural Science Foundation of China (Grant No. 51879218, 51679203) and Fundamental Research Funds for the Central Universities (Grant No. 3102018gxc007, 3102020H HZY030004).

Conflict of interest

The authors declare no conflict of interest.

Notes

Reprinted (adapted) with permission from Chinese Physics B, 2013, 22(7): 074703.

Abbreviations

WT	wavelet transform
PSD	power spectrum density
OWT	orthogonal wavelet transform
PDF	probability density function
CWT	continuous wavelet transform
DWT	discrete wavelet transform
DNS	direct numerical simulation

Nomenclature

$s(t)$	original turbulence signal
$\varphi_{m,n}(t)$	scaling function
a	scale parameter
b	position parameter
m_0	critical scale
$\psi_{m,n}(t)$	wavelet function
$\tilde{s}$	coherent part of the signal
s'	incoherent part of the signal
f	frequency
f_s	sampling frequency
f_c	central frequency of particular wavelet basis
y^+	dimensionless wall distance
$A7,\ \ D1 \sim D7$	detailed signal of each level
v	fluctuating velocity signal
β	correlation parameter

Appendix I: complex wavelet transform

The continuous wavelet transform (CWT) has the drawback of redundancy. As the dilation parameter a and the shift parameter b take continuous values, the resulting CWT is a very redundant representation. Therefore, the discrete wavelet transform was proposed to overcome this problem by setting the scale and shift parameters on a discrete set of basis functions. Their discretization is performed by:

$$a = a_0^j \cdots b = k a_0^j b_0 \cdots \text{for} \cdot j, k \in Z \tag{10}$$

where $a_0 > 1$ is the dilation and $b_0 \neq 0$ is the translation. The family of wavelets can be expressed as:

$$\psi_{j,k}(t) = a_0^{-j/2} \psi\left(a_0^{-j} t - k b_0\right) \tag{11}$$

and the discrete wavelet decomposition of a signal $f(t)$ is:

$$f(t) = \sum_j \sum_k D_f(j,k) \psi_{j,k}(t) \tag{12}$$

where $D_f(j,k)$ is the DWT of the signal $f(t)$. The most widely used dilation and shift parameters are $a = 2$ and $b = 1$.

The basis function set $\left\{\psi_{j,k}\right\}$ should be orthonormal such that:

$$D_f(j,k) = \int_{-\infty}^{\infty} \psi^*_{j,k}(t) f(t) dt = \left\langle \psi_{j,k}(t) f(t) \right\rangle \tag{13}$$

The advantage of the DWT is the multi-resolution analysis ability. Although the standard DWT is powerful, it has three major disadvantages that undermine its applications: shift sensitivity, poor directionality, and absence of phase information.

Complex wavelet transform can be used to overcome these drawbacks. It uses complex-valued filtering and decomposes the signal into real and imaginary parts, which can be used to calculate the amplitude and phase information.

For turbulence analysis, the complex wavelet transform should be used since the modulus of the wavelet coefficients allows characterizing the evolution of the turbulent energy in both the time and frequency domains. The real-valued wavelets will make it difficult to sort out the features of the signal or the wavelet. On the contrary, the complex-valued wavelets can eliminate these spurious oscillations. The complex extension of a real signal $f(t)$ can be expressed as:

$$x(t) = f(t) + jg(t) \tag{14}$$

where $g(t)$ is the Hilbert transform of $f(t)$ and is denoted as $H\{f(t)\}$ and $j = (-1)^{1/2}$. The instantaneous frequency and amplitude of the signal $x(t)$ can then be calculated as:

$$\begin{aligned} &\text{Magnitude of } x(t) = \sqrt{\left(f(t)^2 + g(t)^2\right)} \\ &\text{Angle of } x(t) = \tan^{-1}[g(t)/f(t)] \end{aligned} \tag{15}$$

The complex wavelet transform is able to remove the redundancy for turbulence analysis where the directionality and phase information play important roles.

Author details

Peng Du†, Haibao Hu*† and Xiao Huang
School of Marine Science and Technology, Northwestern Polytechnical University, Xi'an, P.R. China

*Address all correspondence to: huhaibao@nwpu.edu.cn

† These authors are contributed equally.

References

[1] Kowal G, Lazarian A. Velocity field of compressible magnetohydrodynamic turbulence: Wavelet decomposition and mode scalings. The Astrophysical Journal. 2010;**720**(1):742

[2] Xiao-Bing L, Zheng-Qing C, Chao-Qun L. Late-stage vertical structures and eddy motions in a transitional boundary layer. Chinese Physics Letters. 2010;**27**(2):024706

[3] Rinoshika A, Omori H. Orthogonal wavelet analysis of turbulent wakes behind various bluff bodies. Experimental Thermal and Fluid Science. 2011;**35**(7):1231-1238

[4] Rinoshika A, Watanabe S. Orthogonal wavelet decomposition of turbulent structures behind a vehicle external mirror. Experimental Thermal and Fluid Science. 2010;**34**(8): 1389-1397

[5] Okamoto N, Yoshimatsu K, Schneider K, et al. Coherent vortices in high resolution direct numerical simulation of homogeneous isotropic turbulence: A wavelet viewpoint. Physics of Fluids. 2007;**19**(11):115109

[6] De Stefano G, Vasilyev OV. A fully adaptive wavelet-based approach to homogeneous turbulence simulation. Journal of Fluid Mechanics. 2012;**695**: 149-172

[7] Futatani S, Bos WJT, del-Castillo-Negrete D, et al. Coherent vorticity extraction in resistive drift-wave turbulence: Comparison of orthogonal wavelets versus proper orthogonal decomposition. Comptes Rendus Physique. 2011;**12**(2):123-131

[8] de la Llave PM, Cant S, Prosser R. On the use of biorthogonal interpolating wavelets for large-eddy simulation of turbulence. Journal of Computational Physics. 2012;**231**(20):6754-6769

[9] Khujadze G, Schneider K, Oberlack M, et al. Coherent vorticity extraction in turbulent boundary layers using orthogonal wavelets. Journal of Physics: Conference Series. 2011;**318**(2): 022011

[10] Liandrat J, Moret-Bailly F. The wavelet transform-some applications to fluid dynamics and turbulence. European Journal of Mechanics - B/Fluids. 1990;**9**:1-19

[11] Nan J, Jin Z. Detecting multi-scale coherent eddy structures and intermittency in turbulent boundary layer by wavelet analysis. Chinese Physics Letters. 2005;**22**(8):1968

[12] Jian-hua L, Nan J, Zhen-dong W, et al. Multi-scale coherent structures in turbulent boundary layer detected by locally averaged velocity structure functions. Applied Mathematics and Mechanics. 2005;**26**(4):495-504

[13] Kim YH, Cierpka C, Wereley ST. Flow field around a vibrating cantilever: Coherent structure education by continuous wavelet transform and proper orthogonal decomposition. Journal of Fluid Mechanics. 2011;**669**:584-606

[14] Yoshimatsu K, Schneider K, Okamoto N, et al. Intermittency and geometrical statistics of three-dimensional homogeneous magneto-hydrodynamic turbulence: A wavelet viewpoint. Physics of Plasmas. 2011; **18**(9):092304

[15] Baars WJ, Talluru KM, Hutchins N, et al. Wavelet analysis of wall turbulence to study large-scale modulation of small scales. Experiments in Fluids. 2015;**56**(10):188

[16] Camussi R. Coherent structure identification from wavelet analysis of particle image velocimetry data. Experiments in Fluids. 2002;**32**(1):76-86

[17] Longo S. Turbulence under spilling breakers using discrete wavelets. Experiments in Fluids. 2003;**34**(2): 181-191

[18] Arimitsu T, Arimitsu N. Analysis of PDFs for energy transfer rates from 40963 DNS-verification of the scaling relation within MPDFT. Journal of Turbulence. 2011;**12**:N1

[19] Gang D, Shi-Sheng Z, Yang L. Time series prediction using wavelet process neural network. Chinese Physics B. 2008;**17**(6):1998

[20] Asai M, Minagawa M, Nishioka M. The instability and breakdown of a near-wall low-speed streak. Journal of Fluid Mechanics. 2002;**455**:289-314

[21] Chen L, Tang DB. Study on turbulent spots in plane Couette flow. Transactions of Nanjing University of Aeronautics & Astronautics. 2007; **24**(3):211-217

[22] Hu HB, Du P, Huang SH, Wang Y. Extraction and verification of coherent structures in near-wall turbulence. Chinese Physics B. 2013;**22**(7):074703

[23] Huang L, Kemao Q, Pan B, et al. Comparison of Fourier transform, windowed Fourier transform, and wavelet transform methods for phase extraction from a single fringe pattern in fringe projection profilometry. Optics and Lasers in Engineering. 2010;**48**(2):141-148

[24] Canal MR. Comparison of wavelet and short time Fourier transform methods in the analysis of EMG signals. Journal of Medical Systems. 2010;**34**(1): 91-94

[25] Du P, Wen J, Zhang Z, et al. Maintenance of air layer and drag reduction on superhydrophobic surface. Ocean Engineering. 2017;**130**:328-335

[26] Haibao H, Peng D, Feng Z, et al. Effect of hydrophobicity on turbulent boundary layer under water. Experimental Thermal and Fluid Science. 2015;**60**:148-156

[27] Sang YF. A review on the applications of wavelet transform in hydrology time series analysis. Atmospheric Research. 2013;**122**:8-15